Extension of MITC to higher-order beam models and shear locking analysis for compact, thin-walled, and composite structures

(Article begins on next page)

21 August 2022

Extension of MITC to higher-order beam models and shear locking analysis for compact, thin-walled and composite structures

E. Carrera[*], A.G. de Miguel[†], and A. Pagani[‡]

Mul^2 Group

Department of Mechanical and Aerospace Engineering, Politecnico di Torino

Corso Duca degli Abruzzi 24, 10129 Torino, Italy.

[*]Professor of Aerospace Structures and Aeroelasticity, e-mail: erasmo.carrera@polito.it

[†]Marie Curie PhD Student, e-mail: alberto.garcia@polito.it

[‡]Assistant Professor, e-mail: alfonso.pagani@polito.it

Abstract

A class of mixed interpolated beam elements is introduced in this paper under the framework of the Carrera Unified Formulation (CUF) to eliminate the detrimental effects due to shear locking. The Mixed Interpolation of Tensorial Components (MITC) method is adopted to generate locking-free displacement-based beam models using general 1D finite elements. An assumed distribution of the transverse shear strains is employed for the derivation of the virtual work and the full Gauss-Legendre quadrature is used for the numerical computation of all the components of the stiffness matrix. Linear, quadratic and cubic beam elements are developed using the unified formulation and applied to linear static problems including compact, laminated and thin-walled structures. A comprehensive study of how shear locking affects general beam elements when different classical integration schemes are employed is presented, evidencing the outstanding capabilities of the MITC method to overcome this numerical issue. Refined beam theories based on the expansion of pure and generalized displacement variables are implemented making use of Lagrange and Legendre polynomials over the cross-sectional domain, allowing one to capture complex states of stress with a 3D-like accuracy. The numerical examples are compared to analytic, numerical solutions from the literature, and commercial software solutions, whenever it is possible. The efficiency and robustness of the proposed method is demonstrated throughout all the assessments, illustrating that MITC elements are the natural choice to avoid shear locking and showing an unprecedent accuracy in the computation of transverse shear stresses for beam formulations.

Keywords: Finite element method, Shear locking, Refined beam theories, Mixed Interpolation of Tensorial Components, Carrera Unified Formulation.

1 Introduction

During the last decades, the Finite Element Method (FEM) has acquired considerable importance in numerical simulations, specially in the domain of structural analysis and verification. One of the major concerns of structural engineers is the elevated computational costs that are required to study complex geometries and/or boundary conditions, which consumes an important part of the designing process. Researches are working very actively on the development of new formulations based on the use of less demanding 2D/1D finite elements to obtain highly accurate results while minimizing the computational effort. In this context, there are still some challenges to be met in order to obtain effective and reliable tools that can be useful for the engineering analysis.

Since the introduction of FEM, different classes of displacement-based finite formulations have been developed, assessed and extensively employed for engineering analysis. However, it is of common knowledge that finite elements, eventually, undergo numerical problems that make them excessively stiff in bending-dominant problems when thin structures are considered. This stiffening phenomenon is known to as *shear locking* and represents one of the major numerical issues in FEM applications, leading to a sudden and uncontrollable increasing of the shear stiffness. The shear locking problem has been addressed in many works over the last decades and several methods have been presented focusing on alleviating this behaviour (see [1, 2, 3, 4, 5, 6, 7, 8, 9, 10]). Usually, researchers overcome this deficiency by employing well-known numerical 'tricks', such as the reduced integration scheme initially described by Zienkiewicz *et al.* [11]. This method is based on decreasing the order of the numerical integration in certain terms of the stiffness matrix in order to reduce the stiffness of displacement-based elements and, since its introduction, it has been extensively studied in many works [12, 13, 14, 15]. A commonly used variant of the later method is the selective integration technique, which works as a reduced integration for the transverse shear terms whereas a full quadrature is employed for the remaining terms of the stiffness matrix, see [16, 17, 18]. The aforementioned integration schemes improve considerable the convergence rates of the displacement solutions, however, its use leads in some cases to unexpected behaviours due to the appearance of unwanted spurious modes [19].

One of the most successful approaches to tackle this issue is the mixed interpolation of shear strains, introduced by Dvorkin and Bathe [20] and MacNeal [21]. This method, denoted by the former authors to as MITC (Mixed Interpolation of Tensorial Components), is based on the use of *assumed* strain distributions for the derivation of the transverse shear terms, and eventually mebrane terms, of the stiffness matrix of the finite elements. A similar approach was employed in 1956 by Turner et. al [22] for the analysis of complex shell-type aeronautic structures. It should be pointed out that this method might be seen as a selective scheme but, in fact, it works as a full integration of the mixed interpolated element, as stated by Bathe [23] and Bucalem and Bathe [24]. Since its introduction, the MITC approach has been extensively employed on plate and shell formulations in many works, such as Bucalem and Bathe [25], Bathe and Dvorkin [26], Huang and Hinton [27], Park and Stanley [28] and Jang

and Pinsky [29]. However, despite its many advantages, the application of MITC has not received as much attention as far as beam formulations are considered. This paper serves to this purpose and extends MITC methodology to higher-order and hierarchical beam theories.

For many years, classical beam theories, such as those by Euler-Bernoulli [30] and Timoshenko [31], have demonstrated to be an effective tool for many structural problems, although their employability is limited to slender homogeneous beams subjected to bending. It is well known, in fact, that those theories fail in foreseing higher-order phenomena such as out-of-plane warping, torsion, in-plane shear deformations or local effects. In order to overcome the limitations of the classical theories and to capture these effects, many enhanced 1D theories of structures have been proposed. A comprehensive review of the most remarkable contributions in the field can be found in Kapania and Raciti [32, 33] and in Carrera *et al.* [34]. Most of these refined beam models are built based on some physical assumptions, which limit their use to particular classes of problems. In this context, the Carrera Unified Formulation (CUF) [35, 36] was presented as a general structural formulation in which the order and the mathematical assumptions of the theory are introduced as input of the analysis. This methodology allows one to reduce the 3D elasticity problem into 2D or 1D ones by describing the kinematics in a unified manner as an arbitrary expansion of the unknown variables. Its application to the 1D analysis was introduced by Carrera and Giunta [37], who extended the CUF to beam problems using Taylor-like polynomials for the description of the kinematic field, and then enhanced by Carrera and Petrolo [38], who introduced a set of piece-wise expansions based on Lagrange polynomials to capture 3D-like behaviours with an increased accuracy. During the last years, more theories of structure have been developed under the framework of the unified formulation and the capabilities of these models have been extensively assessed in numerous works. However, in many cases, the shear locking phenomenon still have a negative effect in the performance of beam formulations and its elimination is essential if one wants to develop robust locking-free models. Indeed, this issue was addressed in Carrera and Pagani [39], where a constant distribution of the shear strains was assumed to develop classical and Taylor-like locking-free beam models.

The use of the MITC method to eliminate shear locking phenomena on beam elements was initially discussed in the book of Bathe [23]. In this work, the focus is on a two-node Timoshenko beam element and some insights of how general mixed interpolated beam elements should be devised are also provided. More recently, Lee *et al.* [40] proposed a geometry-dependent MITC method to avoid locking on 2-node beam elements dealing with varying section beams. In both works, the shear components of the strain field are computed from the displacements, but interpolated by means of lower-order shape functions. This method leads to a class of locking-free beam elements that are computationally similar to the original ones in that the unknowns of the problem remain only the displacements and the stiffness matrix is formally the same. These characteristics make the MITC approach a suitable candidate to enhance displacement-based beam formulations and a powerful method for the development of highly reliable advanced beam models, extending the 1D structural analysis to a wide

range of geometries and boundary conditions.

The present work presents a systematic generalization of the MITC approach to any-order and class of theory of structure based on 2-node, 3-node and 4-node beam elements. The convergence rates of the solutions are compared against other integration schemes usually employed in commercial softwares, demonstrating the advantages of high-order mixed beam elements to deal with shear locking phenomena. Moreover, MITC beam elements show a remarkable performance in computing the distributions of strains and stresses within the body with an outstanding accuracy for refined beam models. The features of the CUF are exploited in the following to develop theories of structure based on Lagrange-type and Legendre-type polynomials for compact, thin-walled and composite beam structures.

The paper is organized as follows: first, an overview of different variable kinematic CUF models is provided in Section 2. The basis of the finite element method in the framework of 1D CUF is provided in Section 3, with particular attention on the development of MITC beam elements and the derivation of the fundamental nucleus of the stiffness matrix. Several beam and shell-like structures are analyzed with the present 1D model in Section 4, showing the advanced capabilities the higher-order mixed interpolated beam elements on dealing with general problems. Finally, the main conclusions of the work are outlined in Section 5.
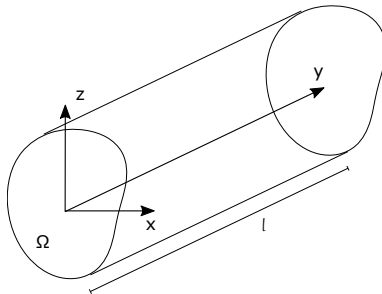
2   CUF beam models

Figure 1: Coordinate system and geometry of a reference beam structure.

Classical beam theories are based upon a number of hypotheses that limit in many cases their accuracy and applicability. For instance, according to the Euler-Bernoulli theory, the cross-section remains plane, rigid and normal to the deformed axis of the beam and the shear deformations are neglected. The Timoshenko model, on the other hand, relaxes the assumption of orthogonality of the cross-section to account for a constant distribution of shear stresses. Consider a Cartesian coordinate system as in Fig. 1. The beam axis coincides with the coordinate y and the cross-section, Ω, lays on the xz-plane. The resulting displacement

field of the Timoshenko theory reads

$$u_x(x, y, z) = u_{x_1}(y)$$
$$u_y(x, y, z) = u_{y_1}(y) + x\phi_z(y) - z\phi_x(y) \qquad (1)$$
$$u_z(x, y, z) = u_{z_1}(y)$$

where u_x, u_y and u_z are the global displacements at any point of the structure, u_{x_1}, u_{y_1} and u_{z_1} are the displacements of the beam axis, and ϕ_z and ϕ_x represent the rotations around the z and x axes. It is of common knowledge that when short, thin-walled or non-homogeneous beam cases are considered, the assumptions adopted to generate these classical theories are not valid anymore, and more refined theories should be employed. For example, the use of high-order kinematic terms is required if stress-free boundary conditions are to be fulfilled, as shown by Reddy [41].

Following these premises, in the framework of the unified formulation, classical theories assumptions are systematically neglected by enriching the kinematic field with an arbitrary number of terms that expand the mechanical variables over the cross-section domain, Ω, with certain functions of the xz-plane. In its compact form it can be expressed as:

$$\mathbf{u}(x, y, z) = F_\tau(x, z)\mathbf{u}_\tau(y) \quad \tau = 1, 2, ..., M \qquad (2)$$

where $\mathbf{u}(x, y, z)$ is the three-dimensional displacement field, $\mathbf{u}_\tau(y)$ is the vector of generalized displacements, M is the number of terms of the kinematic field and $F_\tau(x, z)$ are the so-called expansion functions. It should be noted that, according to the Einstein notation, τ denotes summation. The choice of the theory of structure becomes in this way arbitrary and can be introduced in the structural beam model as an input when defining F_τ. For more information about the CUF methodologies, the reader is referred to the book of Carrera *et al.* [42]. For the sake of completeness, a brief introduction of some of these beam theories is provided in the following.

2.1 Taylor Expansions

Taylor Expansions (TE) are based on the use of 2D series of MacLaurin polynomials of the type $x^i z^j$ to define the interpolating functions over the cross-section, F_τ. For these models, the displacement field is enriched in a hierarchical manner by adding higher-order expansion terms. For instance, the second order model includes 18 generalized displacement variables (displacements and derivatives) as follows:

$$u_x(x, y, z) = u_{x_1}(y) + x\, u_{x_2}(y) + z\, u_{x_3}(y) + x^2\, u_{x_4}(y) + xz\, u_{x_5}(y) + z^2\, u_{x_6}(y)$$
$$u_y(x, y, z) = u_{y_1}(y) + x\, u_{y_2}(y) + z\, u_{y_3}(y) + x^2\, u_{y_4}(y) + xz\, u_{y_5}(y) + z^2\, u_{y_6}(y) \qquad (3)$$
$$u_z(x, y, z) = u_{z_1}(y) + x\, u_{z_2}(y) + z\, u_{z_3}(y) + x^2\, u_{z_4}(y) + xz\, u_{z_5}(y) + z^2\, u_{z_6}(y)$$

where u_{x_τ}, u_{y_τ} and u_{z_τ} ($\tau = 1, ..., 6$) are the generalised displacement unknowns and 1, x, z, x^2, xz and z^2 are the expansion functions. TE models have been extensively used to analyse a broad range of structural problems through the unified formulation, see for instance [43, 44, 45, 39]. It is possible to observe that the classical theories, such as Euler and Timoshenko models, can be considered as particular cases of the first-order TE. For example, considering the constant and linear terms of (Eq. (3)) and imposing $u_{x_2} = u_{x_3} = u_{z_2} = u_{z_2} = 0$, one obtains the displacement field of the Timoshenko model (Eq. (1)), with $\phi_z = u_{y_2}$ and $\phi_x = -u_{y_3}$.

2.2 Lagrange Expansions

Lagrange Expansions (LE) make use of Lagrange-type polynomials to create sets of F_τ functions that are defined in the natural plane and then mapped onto the cross-section surface. In this manner, the section domain is represented by a number of non-local expansions that allow to accurately capture more complex geometries and to enrich the kinematics of the model in particular zones of interest. Different types of expansions can be devised depending on the polynomial order, such as three-node L3, four-node L4, six-node L6 or nine-node L9. A more detailed description can be found in Carrera and Petrolo [38]. As an example, the displacement field of a quadratic L9 model corresponds to that of (Eq. (2)) with the following generic functions:

$$
\begin{aligned}
F_\tau &= \tfrac{1}{4}(r^2 + rr_\tau)(s^2 + ss_\tau) \qquad \tau = 1, 3, 5, 7 \\
F_\tau &= \tfrac{1}{2}s_\tau^2(s^2 - ss_\tau)(1 - r^2) + \tfrac{1}{2}r_\tau^2(r^2 - rr_\tau)(1 - s^2) \qquad \tau = 2, 4, 6, 8 \\
F_\tau &= (1 - r^2)(1 - s^2) \qquad \tau = 9
\end{aligned}
\tag{4}
$$

where r and s are the coordinates of the natural plane $[-1,1] \times [-1,1]$ and r_τ and s_τ are the position of the nodes. This class of beam models have been successfully applied to many different fields, such as composite laminates [46], aerospace structures [47, 48], civil constructions [49, 50], and marine ship hulls [51].

2.3 Hierarchical Legendre Expansions

In Hierarchical Legendre Expansions, also denoted to as HLE, the F_τ generic expansions are defined from a set of hierarchical functions derived from Legendre polynomials. HLE models were recently introduced in the work of Carrera *et al.* [52] and its main feature is that they combine the hierarchy in the structure of the kinematic terms (as for TE) with a non-local distribution of the mechanical unknowns over the cross-section domain (as for LE). More specifically, this class of models makes use of three types of expansion polynomials: vertex, side and internal.

Vertex expansions

$$F_\tau = \frac{1}{4}(1 - r_\tau r)(1 - s_\tau s) \qquad \tau = 1, 2, 3, 4 \tag{5}$$

where r and s vary over the natural frame between -1 and $+1$, and r_τ and s_τ represent the vertex coordinates of the quadrilateral domain.

Side expansions

$$F_\tau(r, s) = \frac{1}{2}(1 - s)\phi_p(r) \qquad \tau = 5, 9, 13, 18, ... \tag{6}$$

$$F_\tau(r, s) = \frac{1}{2}(1 + r)\phi_p(s) \qquad \tau = 6, 10, 14, 19, ... \tag{7}$$

$$F_\tau(r, s) = \frac{1}{2}(1 + s)\phi_p(r) \qquad \tau = 7, 11, 15, 20, ... \tag{8}$$

$$F_\tau(r, s) = \frac{1}{2}(1 - r)\phi_p(s) \qquad \tau = 8, 14, 16, 21, ... \tag{9}$$

where ϕ_p corresponds to the one-dimensional internal Legendre-type modes, as presented in the book of Szabó and Babuška [53]. They are defined for $p \geq 2$, where p is the polynomial order of the beam theory.

Internal expansions Introduced for $p \geq 4$, they vanish at all the edges of the quadrilateral domain. They sum $(p-2)(p-3)/2$ internal polynomials in total. For the sake of clarity, the sixth-order polynomial set is included here:

$$F_{28}(r, s) = \phi_4(r)\phi_2(s) \tag{10}$$

$$F_{29}(r, s) = \phi_3(r)\phi_3(s) \tag{11}$$

$$F_{30}(r, s) = \phi_2(r)\phi_4(s) \tag{12}$$

HLE theories have been employed for the analysis of laminated structures [54] and further extended to develop geometrically-exact beam models through the blending mapping technique [55].

3 Finite element formulation

3.1 Preliminaries

The strain and stress second-order tensors can be expressed the form of six-term column vectors. For the purposes of this work, these vectors are split in bending components (subscript

B) and transverse shear components (subscript S), as:

$$\boldsymbol{\varepsilon}_B = \{\varepsilon_{yy}\ \varepsilon_{xx}\ \varepsilon_{zz}\ \varepsilon_{xz}\}^T \quad \boldsymbol{\varepsilon}_S = \{\varepsilon_{yz}\ \varepsilon_{xy}\}^T$$
$$\boldsymbol{\sigma}_B = \{\sigma_{yy}\ \sigma_{xx}\ \sigma_{zz}\ \sigma_{xz}\}^T \quad \boldsymbol{\sigma}_S = \{\sigma_{yz}\ \sigma_{xy}\}^T \tag{13}$$

In linear analyses, the geometrical relations between strains and displacements, following the present nomenclature, read:

$$\boldsymbol{\varepsilon}_B = \boldsymbol{D}_B\,\boldsymbol{u} = (\boldsymbol{D}_{B_y} + \boldsymbol{D}_{B_\Omega})\,\boldsymbol{u}$$
$$\boldsymbol{\varepsilon}_S = \boldsymbol{D}_S\,\boldsymbol{u} = (\boldsymbol{D}_{S_y} + \boldsymbol{D}_{S_\Omega})\,\boldsymbol{u} \tag{14}$$

where the differential operators $\boldsymbol{D}_B$ and $\boldsymbol{D}_S$ can be conveniently defined as

$$\boldsymbol{D}_{B_y} = \begin{bmatrix} 0 & \frac{\partial(\bullet)}{\partial y} & 0 \\ 0 & 0 & 0 \\ 0 & 0 & 0 \\ 0 & 0 & 0 \end{bmatrix} \quad \boldsymbol{D}_{B_\Omega} = \begin{bmatrix} 0 & 0 & 0 \\ \frac{\partial(\bullet)}{\partial x} & 0 & 0 \\ 0 & 0 & \frac{\partial(\bullet)}{\partial z} \\ \frac{\partial(\bullet)}{\partial z} & 0 & \frac{\partial(\bullet)}{\partial x} \end{bmatrix}$$
$$\boldsymbol{D}_{S_y} = \begin{bmatrix} 0 & 0 & \frac{\partial(\bullet)}{\partial y} \\ \frac{\partial(\bullet)}{\partial y} & 0 & 0 \end{bmatrix} \quad \boldsymbol{D}_{S_\Omega} = \begin{bmatrix} 0 & \frac{\partial(\bullet)}{\partial z} & 0 \\ 0 & \frac{\partial(\bullet)}{\partial x} & 0 \end{bmatrix} \tag{15}$$

On the other hand, the stress components are obtained making use of the the constitutive laws as follows:

$$\left\{ \begin{array}{c} \boldsymbol{\sigma}_B \\ \boldsymbol{\sigma}_S \end{array} \right\} = \left[\begin{array}{cc} \tilde{\mathbf{C}}_{BB} & \tilde{\mathbf{C}}_{BS} \\ \tilde{\mathbf{C}}_{SB} & \tilde{\mathbf{C}}_{SS} \end{array} \right] \left\{ \begin{array}{c} \boldsymbol{\varepsilon}_B \\ \boldsymbol{\varepsilon}_S \end{array} \right\} \tag{16}$$

where the transformed material matrix, $\tilde{\mathbf{C}}$, contains the material characteristics in the global coordinate frame (see Fig. 1) and has been also regrouped in bending and transverse shear terms. If fiber-reinforced laminas are considered, the material matrices are:

$$\tilde{\mathbf{C}}_{BB} = \begin{bmatrix} \tilde{C}_{33} & \tilde{C}_{23} & \tilde{C}_{13} & 0 \\ \tilde{C}_{23} & \tilde{C}_{22} & \tilde{C}_{12} & 0 \\ \tilde{C}_{13} & \tilde{C}_{12} & \tilde{C}_{11} & 0 \\ 0 & 0 & 0 & \tilde{C}_{44} \end{bmatrix} \quad \tilde{\mathbf{C}}_{BS} = \tilde{\mathbf{C}}_{SB}^T = \begin{bmatrix} 0 & \tilde{C}_{36} \\ 0 & \tilde{C}_{26} \\ 0 & \tilde{C}_{16} \\ \tilde{C}_{45} & 0 \end{bmatrix} \quad \tilde{\mathbf{C}}_{SS} = \begin{bmatrix} \tilde{C}_{55} & 0 \\ 0 & \tilde{C}_{66} \end{bmatrix} \tag{17}$$

The material coefficients, $\tilde{C}_{ij}$, depend on the Young's modulus, the Poisson ratio and the orientation of the fibers. Their explicit expressions are not incuded here for the sake of brevity, but they can be found in many works in the literature, see for instance the book of Reddy [56].

3.2 MITC elements

As in classical finite element formulations, in the CUF framework the problem unknowns are allocated at the structural nodes. The nodal displacement vector is expressed as:

$$\boldsymbol{u}_{\tau i} = \{u_{x_{\tau i}} \ u_{y_{\tau i}} \ u_{z_{\tau i}}\}^T \quad \tau = 1, .., M; \ i = 1, ..., n_{node} \tag{18}$$

where M is the number of terms of the expansion and n_{node} stands for the number of nodes per element. Then, the displacement variables are interpolated along the beam axis by means of conventional 1D shape functions, N_i:

$$\mathbf{u}_\tau(y) = N_i(y)\mathbf{u}_{\tau i} \quad i = 1, ..., n_{node} \tag{19}$$

Standard Lagrangian beam elements including two, three and four nodes are considered for the purposes of the present work. The expressions of the interpolating functions, N_i, of these elements are, respectively:

$$N_1 = \tfrac{1}{2}(1 - \xi), \quad N_2 = \tfrac{1}{2}(1 + \xi), \quad \begin{cases} \xi_1 = -1 \\ \xi_2 = +1 \end{cases} \tag{20}$$

$$N_1 = \tfrac{1}{2}\xi(\xi - 1), \quad N_2 = \tfrac{1}{2}\xi(\xi + 1), \quad N_3 = -(1 + \xi)(1 - \xi), \quad \begin{cases} \xi_1 = -1 \\ \xi_2 = +1 \\ \xi_3 = 0 \end{cases} \tag{21}$$

$$N_1 = -\tfrac{9}{16}(\xi + \tfrac{1}{3})(\xi - \tfrac{1}{3})(\xi - 1), \quad N_2 = \tfrac{9}{16}(\xi + \tfrac{1}{3})(\xi - \tfrac{1}{3})(\xi + 1),$$
$$N_3 = +\tfrac{27}{16}(\xi + 1)(\xi - \tfrac{1}{3})(\xi - 1), \quad N_4 = -\tfrac{27}{16}(\xi + 1)(r + \tfrac{1}{3})(\xi - 1), \quad \begin{cases} \xi_1 = -1 \\ \xi_2 = +1 \\ \xi_3 = -\tfrac{1}{3} \\ \xi_4 = +\tfrac{1}{3} \end{cases} \tag{22}$$

where the natural coordinate, ξ, goes from -1 to $+1$ and ξ_i denotes the position of the nodes in the natural coordinate system of the element.

In displacement-based finite formulations, the strain components are obtained directly from the displacement solutions through the geometrical relations (Eq. (14)). Making use of the CUF kinematic approximation (Eq. (2)) and the FEM interpolation (Eq. (19)), the bending and shear strain components can be computed:

$$\begin{aligned} \varepsilon_B &= F_\tau(\boldsymbol{D}_{B_y} N_i \mathbf{I})\mathbf{u}_{\tau i} + (\boldsymbol{D}_{B_\Omega} F_\tau \mathbf{I})N_i \mathbf{u}_{\tau i} \\ \varepsilon_S &= F_\tau(\boldsymbol{D}_{S_y} N_i \mathbf{I})\mathbf{u}_{\tau i} + (\boldsymbol{D}_{S_\Omega} F_\tau \mathbf{I})N_i \mathbf{u}_{\tau i} \end{aligned} \tag{23}$$

being $\mathbf{I}$ the 3×3 identity matrix.

Conventional finite elements are often too stiff due to shear locking phenomena, and in particular when low-order shape functions are used. The MITC method tackles this numerical deficiency by interpolating separately the displacements and the transverse shear strains. According to the MITC premises, the transverse shear strains along the beam element are
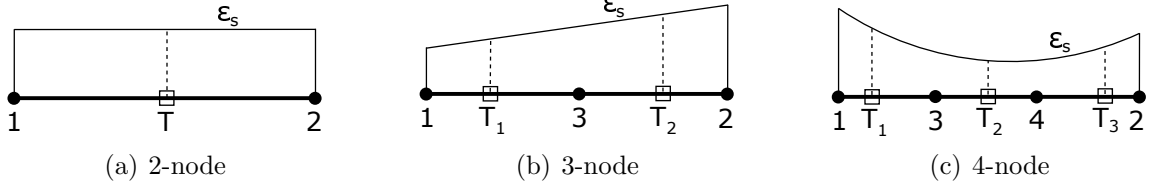
Figure 2: MITC element interpolations of shear strains.

assumed as:

$$\bar{\boldsymbol{\varepsilon}}_S = \bar{N}_m \, \boldsymbol{\varepsilon}_{S_m} \qquad m = 1, ..., n_{node} - 1 \tag{24}$$

where m denotes summation over a set of points along the natural coordinate ξ, denoted to as *tying points*. These points are used to tie the interpolations of the displacements with the assumed strains. $\boldsymbol{\varepsilon}_{S_m}$ is the transverse shear strains vector computed at the tying points m by means of Eq. (23). Accordingly, the assumed shear strains vector, $\bar{\boldsymbol{\varepsilon}}_S$, is calculated using one tying point for 2-node elements, two for 3-node elements and three for 4-node elements, as shown in Fig. 2. One can see that transverse shear strains are assumed to be constant, linear or quadratically distributed, respectively. For the sake of completeness, the assumed interpolating functions, $\bar{N}_m$, are given in the following for two-, three-, and four-noded finite elements. Respectively,

$$\bar{N}_1 = 1, \qquad \xi_T = 0 \tag{25}$$

$$\bar{N}_1 = -\tfrac{1}{2}\sqrt{3}(\xi - \tfrac{1}{\sqrt{3}}), \quad \bar{N}_2 = \tfrac{1}{2}\sqrt{3}(\xi + \tfrac{1}{\sqrt{3}}), \quad \begin{cases} \xi_{T_1} = -\frac{1}{\sqrt{3}} \\ \xi_{T_2} = \frac{1}{\sqrt{3}} \end{cases} \tag{26}$$

$$\bar{N}_1 = \tfrac{5}{6}\xi(\xi - \sqrt{\tfrac{3}{5}}), \quad \bar{N}_2 = -\tfrac{5}{3}(\xi - \sqrt{\tfrac{3}{5}})(\xi + \sqrt{\tfrac{3}{5}}), \bar{N}_3 = \tfrac{5}{6}\xi(\xi + \sqrt{\tfrac{3}{5}}), \quad \begin{cases} \xi_{T_1} = -\sqrt{\tfrac{3}{5}} \\ \xi_{T_2} = 0 \\ \xi_{T_3} = \sqrt{\tfrac{3}{5}} \end{cases} \tag{27}$$

where ξ_{T_m} denotes the position of the tying points in the natural reference frame of the beam element. In the present work, the lector can verify that their location coincide with the Gauss points, although they are actually called Barlow points [57], which are known to provide the best accuracy when computing the strain values for these elements.

Now, introducing the expression of the shear strains of Eq. (23) into Eq. (24), one obtains:

$$\bar{\boldsymbol{\varepsilon}}_S = \bar{N}_m F_\tau (\boldsymbol{D}_{S_y} N_i \mathbf{I})_m \mathbf{u}_{\tau i} \ + \ \bar{N}_m (\boldsymbol{D}_{S_\Omega} F_\tau \mathbf{I}) N_{i_m} \mathbf{u}_{\tau i} \tag{28}$$

where N_{i_m} is the value that the shape function N_i takes at the tying point m in the natural coordinate system, and $(\boldsymbol{D}_{S_y} N_i \mathbf{I})_m$ refers to the value of the shape function derivatives

evaluated also at the tying points. The stress field is then computed from Eq. (16), obtaining:

$$\begin{aligned}
\bar{\boldsymbol{\sigma}}_B = \ & \tilde{\mathbf{C}}_{BB}\left[F_\tau(\boldsymbol{D}_{B_y}N_i\mathbf{I})\mathbf{u}_{\tau i} + (\boldsymbol{D}_{B_\Omega}F_\tau\mathbf{I})N_i\mathbf{u}_{\tau i}\right] \\
& + \tilde{\mathbf{C}}_{BS}\left[\bar{N}_m F_\tau(\boldsymbol{D}_{S_y}N_i\mathbf{I})_m\mathbf{u}_{\tau i} + \bar{N}_m(\boldsymbol{D}_{S_\Omega}F_\tau\mathbf{I})N_{i_m}\mathbf{u}_{\tau i}\right] \\
\bar{\boldsymbol{\sigma}}_S = \ & \tilde{\mathbf{C}}_{SB}\left[F_\tau(\boldsymbol{D}_{B_y}N_i\mathbf{I})\mathbf{u}_{\tau i} + (\boldsymbol{D}_{B_\Omega}F_\tau\mathbf{I})N_i\mathbf{u}_{\tau i}\right] \\
& + \tilde{\mathbf{C}}_{SS}\left[\bar{N}_m F_\tau(\boldsymbol{D}_{S_y}N_i\mathbf{I})_m\mathbf{u}_{\tau i} + \bar{N}_m(\boldsymbol{D}_{S_\Omega}F_\tau\mathbf{I})N_{i_m}\mathbf{u}_{\tau i}\right]
\end{aligned} \tag{29}$$

3.3 Stiffness matrix

The arrays of the structural problem, i.e stiffness matrix and loading vector, are derived from the principle of virtual displacements, which for static analyses can be written as:

$$\delta L_{\text{int}} = \delta L_{\text{ext}} \tag{30}$$

It states that the virtual variation of the internal work, L_{int}, must be equal to the virtual variation of the external work, L_{ext}. The former term is equivalent to the elastic strain energy, which for the purposes of the MITC approach can be expressed as

$$\delta L_{int} = \int_l \int_\Omega \delta\boldsymbol{\varepsilon}^T\boldsymbol{\sigma}\,d\Omega\,dy = \int_l \int_\Omega (\delta\boldsymbol{\varepsilon}_B^T\,\bar{\boldsymbol{\sigma}}_B + \delta\bar{\boldsymbol{\varepsilon}}_S^T\,\bar{\boldsymbol{\sigma}}_S)\,d\Omega\,dy \tag{31}$$

where Ω and l are the surface of the cross-section and the length of the beam, respectively (see Fig. 1). Regarding the external work, L_{ext}, it can be derived for the case of a generic concentrated load $\mathbf{P} = (P_x \quad P_y \quad P_z)$, with no loss of generality, as follows:

$$\delta L_{ext} = \boldsymbol{P}\,\delta\boldsymbol{u}^T \tag{32}$$

Now introducing both bending and shear stresses of Eq. (29), the assumed transverse shear strains, $\bar{\boldsymbol{\varepsilon}}_S$, of Eq. (28) and the bending strains, $\boldsymbol{\varepsilon}_B$, of Eq. (23) into Eq. (31), and the CUF notation to Eq. (32), one obtains

$$\begin{aligned}
\delta L_{\text{int}} &= \delta\mathbf{u}_{\tau i}^T\mathbf{K}^{\tau sij}\mathbf{u}_{sj} \\
\delta L_{\text{ext}} &= F_\tau N_i\boldsymbol{P}\delta\mathbf{u}_{\tau i}^T
\end{aligned} \tag{33}$$

where $\mathbf{K}^{\tau sij}$ is the 3×3 building block of the MITC stiffness matrix, denoted to as fundamental nucleus. Note that indexes i and τ of Eq. (29) have been substituted for s and j to be formally coherent with Eq. (31). In the case of monoclinic materials materials (e.g. fiber-reinforced laminae with arbitrary orientations in the xy-plane), the nine components of

the fundamental nucleus are:

$$
\begin{aligned}
K_{xx}^{\tau s i j} &= \widetilde{C}_{22} \int_l N_i N_j \, dy \, E_{\tau,x s,x} \; + \; \widetilde{C}_{44} \int_l N_i N_j \, dy \, E_{\tau,z s,z} \; + \; \widetilde{C}_{26} \int_l N_i (N_n N_{(j,y)_n}) \, dy \, E_{\tau,x s} \\
&\quad + \widetilde{C}_{26} \int_l (N_m N_{(i,y)_m}) N_j \, dy \, E_{\tau s,x} \; + \; \widetilde{C}_{66} \int_l (N_m N_{(i,y)_m})(N_n N_{(j,y)_n}) \, dy \, E_{\tau s} \\
K_{xy}^{\tau s i j} &= \widetilde{C}_{23} \int_l N_i N_{j,y} \, dy \, E_{\tau,x s} \; + \; \widetilde{C}_{45} \int_l N_i (N_n N_{j_n}) \, dy \, E_{\tau,z s,z} \; + \; \widetilde{C}_{26} \int_l N_i (N_n N_{j_n}) \, dy \, E_{\tau,x s,x} \\
&\quad + \widetilde{C}_{36} \int_l (N_m N_{(i,y)_m}) N_j \, dy \, E_{\tau s} \; + \; \widetilde{C}_{66} \int_l (N_m N_{(i,y)_m})(N_n N_{j_n}) \, E_{\tau s,x} \\
K_{xz}^{\tau s i j} &= \widetilde{C}_{12} \int_l N_i N_j \, dy \, E_{\tau,x s,z} \; + \; \widetilde{C}_{44} \int_l N_i N_j \, dy \, E_{\tau,z s,x} \; + \; \widetilde{C}_{45} \int_l N_i (N_n N_{(j,y)_n}) \, E_{\tau,z s} \\
&\quad + \widetilde{C}_{16} \int_l (N_m N_{(i,y)_m}) N_j \, E_{\tau s,z} \\
K_{yx}^{\tau s i j} &= \widetilde{C}_{23} \int_l N_{i,y} N_j \, dy \, E_{\tau s,x} \; + \; \widetilde{C}_{45} \int_l (N_m N_{i_m}) N_j \, dy \, E_{\tau,z s,z} \; + \; \widetilde{C}_{26} \int_l (N_m N_{i_m}) N_j \, dy \, E_{\tau,x s,x} \\
&\quad + \widetilde{C}_{36} \int_l N_{i,y} (N_n N_{(j,y)_n}) \, dy \, E_{\tau s} \; + \; \widetilde{C}_{66} \int_l (N_m N_{i_m})(N_n N_{(j,y)_n}) \, dy \, E_{\tau,x s} \\
K_{yy}^{\tau s i j} &= \widetilde{C}_{33} \int_l N_{i,y} N_{j,y} \, dy \, E_{\tau s} \; + \; \widetilde{C}_{36} \int_l (N_m N_{i_m}) N_{j,y} \, dy \, E_{\tau,x s} \; + \; \widetilde{C}_{36} \int_l N_{i,y} (N_n N_{j_n}) \, E_{\tau s,x} \\
&\quad + \widetilde{C}_{55} \int_l (N_m N_{i_m})(N_n N_{j_n}) \, dy \, E_{\tau,z s,z} \; + \; \widetilde{C}_{66} \int_l (N_m N_{i_m})(N_n N_{j_n}) \, dy \, E_{\tau,x s,x} \\
K_{yz}^{\tau s i j} &= \widetilde{C}_{13} \int_l N_{i,y} N_j \, dy \, E_{\tau s,z} \; + \; \widetilde{C}_{55} \int_l (N_m N_{i_m})(N_n N_{(j,y)_n}) \, dy \, E_{\tau,z s} \\
&\quad + \widetilde{C}_{45} \int_l (N_m N_{i_m}) N_j \, dy \, E_{\tau,z s,x} \; + \; \widetilde{C}_{16} \int_l (N_m N_{i_m}) N_j \, dy \, E_{\tau,x s,z} \\
K_{zx}^{\tau s i j} &= \widetilde{C}_{12} \int_l N_i N_j \, dy \, E_{\tau,z s,x} \; + \; \widetilde{C}_{44} \int_l N_i N_j \, dy \, E_{\tau,x s,z} \; + \; \widetilde{C}_{45} \int_l (N_m N_{(i,y)_m}) N_j \, dy \, E_{\tau s,z} \\
&\quad + \widetilde{C}_{16} \int_l N_i (N_n N_{(j,y)_n}) \, dy \, E_{\tau,z s} \\
K_{zy}^{\tau s i j} &= \widetilde{C}_{13} \int_l N_i N_j \, dy \, E_{\tau,z s} \; + \; \widetilde{C}_{55} \int_l (N_m N_{(i,y)_m})(N_n N_{j_n}) \, dy \, E_{\tau s,z} \\
&\quad + \widetilde{C}_{45} \int_l N_i (N_n N_{(j,y)_n}) \, dy \, E_{\tau,x s,z} \; + \; \widetilde{C}_{16} \int_l N_i (N_n N_{(j,y)_n}) \, dy \, E_{\tau,z s,x} \\
K_{zz}^{\tau s i j} &= \widetilde{C}_{11} \int_l N_i N_j \, dy \, E_{\tau,z s,z} \; + \; \widetilde{C}_{44} \int_l N_i N_j \, dy \, E_{\tau,x s,x} \; + \; \widetilde{C}_{45} \int_l N_i (N_n N_{(j,y)_n}) \, dy \, E_{\tau,x s} \\
&\quad + \widetilde{C}_{55} \int_l (N_m N_{(i,y)_m})(N_n N_{(j,y)_n}) \, dy \, E_{\tau s} \; + \; \widetilde{C}_{45} \int_l (N_m N_{(i,y)_m}) N_j \, dy \, E_{\tau s,x}
\end{aligned}
$$

(34)

where the (i,j) subscripts correspond to the element nodes and (τ, s) to the expansion terms of the beam theory. The comma indicates partial derivative with respect to x, y and z. On the other hand, the (m, n) subscripts refer to the tying points. Using this notation, N_m stands for the m-th assumed interpolating function of the shear strains, whereas $N_{(i,y)_m}$ refers to the derivative with respect to y of the standard shape function N_i evaluated at the tying point m, or, equivalently, $N_{i,y}(T_m)$. For the shake of simplicity, the integrals over the cross-section domain, Ω, are represented by E terms, whose explicit expressions can be found in Appendix A. For further information on the construction of the problem arrays for general cases, the reader is refered to the book of Carrera *et al.* [42].

For the obtention of locking-free MITC elements, the integrals of the shear terms in Eq. (34) account for the assumed interpolating functions, N_m and N_n, which are one order inferior to those of the bending components. In this manner, a reduced-order set of shape functions is employed to approximate the transverse shear strains while a full integration is performed for all the stiffness components, avoiding the numerical issues that may raise when reduced integration schemes are employed. As a final remark, one can notice that in the CUF framework, any beam model, classical to higher-order, can be straightforwardly formulated by only expanding appropriately the fundamental nucleus on $(i, j) = 1, ..., n_{node}$ and $(\tau, s) = 1, ..., M$ to obtain the stiffness matrix. In fact, the formal expressions of the fundamental nucleus are independent of the order and class of theory of structure, represented by F_τ, which can be automatically introduced as an user input of the problem.

4   Numerical results

The capabilities of the present formulation are assessed through several numerical examples. First, a cantilever square beam, for which an analytical solution is available, is solved using a single beam element of different configurations and the performance of the MITC method is compared against classical integration schemes. Secondly, the proposed beam elements are tested under different loading cases, including bending, torsion and bending-torsion. Then, the advantages of the MITC method for the accurate analysis of laminated components through layer-wise models are presented. Finally, a thin-walled L-angle beam is considered and the solutions are compared to 1D, 2D and 3D commercial models, showing the remarkable performance of the present finite element when implemented with high-order theories of structure.

4.1   Single beam element

A simple beam problem is considered first to test the bending and shear capabilities of Lagrange-class 1D elements in a relatively short structure. The example consists in a cantilever beam loaded at the free edge with a vertical point load, see Fig. 3. The dimension of the square cross-section, b, is equal to 0.1 m, whereas the length, L, is equal to 1 m, being the slenderness ratio, L/h, as high as 10. A single beam element is used to solve the numerical problem and to assess the capabilities of the MITC method. The vertical load has a magnitude of -100 N and it is applied at the center of the cross-section. The material properties correspond to an Aluminum alloy, with the following characteristics: Young modulus, E, equal to 75 GPa and the Poisson ratio, ν, equal to 0.33. Bilinear and quadratic beam theories are considered by employing L4 and L9 Lagrange-based expansions as F_τ.

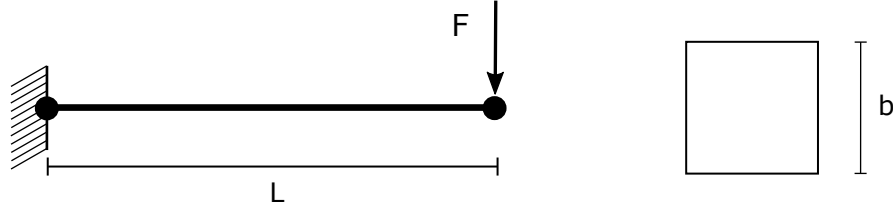The analytical solution of this problem can be obtained from the classical beam theories.

Figure 3: A single two-node beam element representing a cantilever beam.

Using the Timoshenko's theory, the vertical displacementa at the tip results:

$$u = u_{z_b} + u_{z_s} = \frac{F_z L^3}{3EI} + \frac{F_z L}{AG} = -5.369 \times 10^{-5} \ m, \tag{35}$$

On the other hand, the shear stress distribution along the z-axis is obtained from the following formula:

$$\sigma_{yz}(z) = -\frac{F_z S_x(z)}{Ib}, \tag{36}$$

where $S_x(z) = \int_A z dA$ correspond to the first momentum of area and I is the moment of inertia of the section. Accordingly to Eq. (36), the maximum shear stress is located in $z = 0$ and it is given by:

$$\sigma_{yz}(z = 0) = -\frac{3F_z}{2A} = -1.500 \times 10^4 \ Pa. \tag{37}$$

The attention is focused here on how the shear locking affects beam elements derived from different integration schemes. Four integration methods have been considered: full, reduced, selective reduced and mixed integration (MITC), which have already been introduced in Section 1. The first three classes are well-known in the FEM field and they are extensively employed in commercial softwares. Table 1 shows the results of vertical displacements and transverse stresses case for linear, quadratic and cubic beam elements (B2, B3 and B4, respectively). The displacements are evaluated at the center of the tip cross-section, whereas the shear stresses, σ_{yz}, are measured also at the center of the section correspondent to each one of the nodes of the elements. In addition, the distribution of shear stresses along the beam axis for the linear L4 model is shown for all the models considered in Fig. 4.

Some remarks can be outlined from these results:

- Obviously, the higher is the number of beam nodes, i.e. the polynomial order of the shape functions, the better is the approximation in terms of vertical displacements. This applies also to the polynomial order of the expansion functions of the cross-section domain. In fact, the L9 model (quadratic) computes higher displacements than the L4 model (bilinear).

- All beam elements show locking when full integration schemes are employed. This deficiency is more clear for the linear 2-node element, in which the values of displacements are close to zero at the tip. The use of reduced integration mitigates the issue, leading to a less stiff behaviour in particular when three and four-node elements are chosen.

15

		L4 model					L9 model				
		$u_z \times 10^5$ m	$\sigma_{yz} \times 10^{-4}$ Pa				$u_z \times 10^5$ m	$\sigma_{yz} \times 10^{-4}$ Pa			
		y = L	Node 1	Node 2	Node 3	Node 4	y = L	Node 1	Node 2	Node 3	Node 4
B2	Full	-0.138	-3.902	1.902	-	-	-0.139	-3.915	1.910	-	-
	Reduced	-3.382	-95.367	93.367	-	-	-4.035	-113.770	111.684	-	-
	Selective	-3.193	-90.037	88.037	-	-	-3.606	-101.664	99.605	-	-
	MITC	-3.193	-1.000	-1.000	-	-	-3.606	-1.029	-1.029	-	-
B3	Full	-3.424	-4.935	0.967	-4.935	-	-3.942	-4.667	0.810	-4.603	-
	Reduced	-4.492	-32.355	14.678	-32.355	-	-5.363	-38.485	17.687	-38.056	-
	Selective	-4.175	-27.889	12.445	-27.889	-	-4.663	-28.628	12.771	-28.431	-
	MITC	-4.175	-1.000	-1.000	-1.000	-	-4.663	-1.094	-0.996	-0.898	-
B4	Full	-4.311	-0.289	-1.290	-0.710	-1.711	-4.950	0.386	-1.582	-0.357	-2.581
	Reduced	-4.488	-0.841	-1.065	-0.935	-1.159	-5.359	-0.849	-1.135	-0.694	-2.005
	Selective	-4.319	1.497	-2.017	0.017	-3.497	-4.988	4.334	-3.248	1.327	6.659
	MITC	-4.319	-1.000	-1.000	-1.000	-1.000	-4.988	-1.228	-0.982	-0.939	-1.097

Table 1: Results of displacements and shear stresses, σ_{yz}, for various models and integration schemes at the center point of the cross-section.
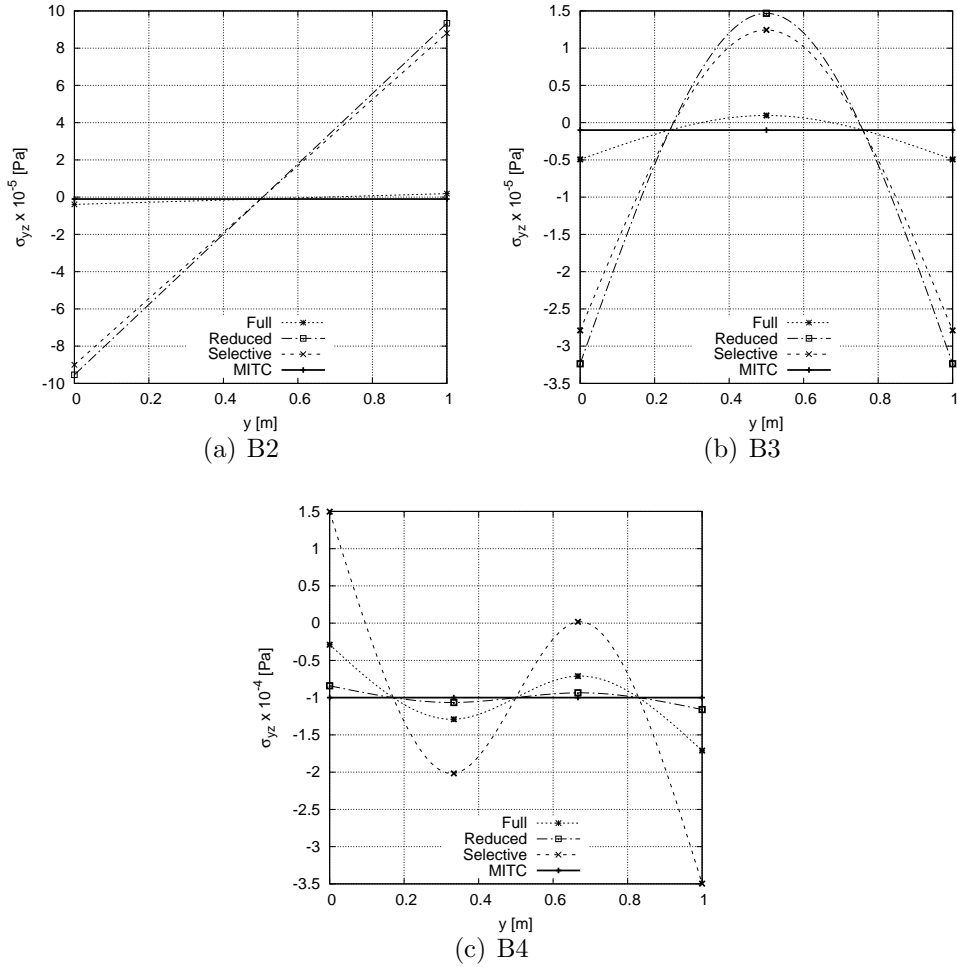

(a) B2

(b) B3

(c) B4

Figure 4: Shear stresses, σ_{yz}, along the beam axis for a L4 model.

Selective and MITC integration schemes provide the same solutions in terms of vertical displacements.

- As it is commonly known, high-order finite elements are a good choice to reduce the diffusion of numerical errors. In the present analysis, it has been demonstrated that its use is indicated to overcome the shear locking.

- Regarding the stress solutions, Fig. 4 shows that MITC elements are the only ones that compute constant values of σ_{yz} along the axis, which, according to the theory of elasticity, is the expected behavior for pure-bending problems. On the other hand, highly oscillating solutions are obtained when other integration methods are employed. The error in the shear stress solutions for reduced integration methods can be of orders of magnitude, which prevents its use if one wants to obtain reliable solutions of the complete stress field.

Equation (36) suggests that the distribution of shear stresses along the z-direction should be quadratic. Therefore, if one wants to approximate the stress field with enough accuracy it is necessary to enrich the kinematic field with higher-order terms. This can be accomplished, for instance, by employing refined HLE theories of structure. The higher-order polynomial expansions employed by HLE models, together with the mixed interpolation of tensorial components, allow us to represent any distribution of strains/stresses over the cross-section of the structure. Figure 5 shows the distribution of shear stresses through the thickness (z-axis) for a four-node MITC element at 33 % of the length, coinciding with the second beam node, employing different HLE models of increasing order. As expected, linear (HL1) and quadratic (HL2) expansions do not respect the stress-free conditions at the boundaries. On the other hand, higher-order expansions are in good agreement the solutions calculated from the analytical expression.

4.2 Square cross-section beam under bending, torsion and bending-torsion loadings

A similar structure of the previous section is considered and meshed with an increasing number of finite elements to study the convergence rates of the different integration methods. The length, L, is equal to 2 m, and the section dimension, b, is 0.2 m. For the second analysis case, a vertical point force is applied at the free end, being its magnitude $F_z = 200$ N. A quadratic L9 model is chosen for the cross-sectional expansions and linear B2 finite elements are employed to mesh the beam axis. The results, shown in Fig. 6, assess the faster convergence in terms of displacements of the reduced integration scheme. The full integration lead to very stiff elements that show much slower rates of convergence. It is also remarkable how selective integration solutions adopt exactly the same trend that MITC elements, although, as it has been demonstrated before, they lack on representing the correct shear components of stresses.
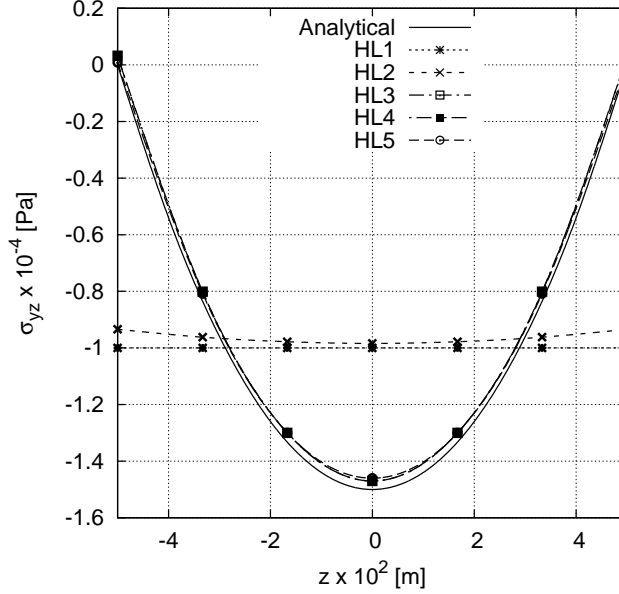
Figure 5: Shear stresses, σ_{yz}, along the z-axis for the MITC4 beam model and various hierarchical expansions at y = L/3.

Based on this results, a conservative choice of 100 2-node MITC elements is used for the next examples of this assessment.

The focus is now centered on the assessment of the accuracy of MITC high-order beam elements for different load cases. First, a torsional load is applied at the tip section by means of two opposite point loads of magnitude $F_z = 50$ N, as it is shown in Fig. 7 (a). The results in terms of displacements and shear stresses are addressed in Table 2. The number of degrees of freedom of each model is also included in the last column. Solutions from LE and HLE models are presented and compared with other results from Carrera and Pagani [39]. The analytical solutions for the displacement and maximum shear stress have been calculated from the well-known formulas [58]:

$$\theta = \frac{TL}{GJ_t}; \qquad \sigma_{yz} \simeq \frac{T}{0.208b^3} \tag{38}$$

where θ is the torsion angle, T the torque load, G the shear modulus and J_t the torsional moment of inertia, approximated as $J_t \simeq 0.1406b^4$. It is clear from Table 2 that at least a third order expansion on the cross-section plane is required for CUF models to compute accurately the correct displacement field due to the warping phenomena that occurs under torsional loads. In fact, Lagrange-type models L4 and L9 do not provide good results. It should be mentioned that this issue could be solved by using higher-order Lagrange polynomials or by incrementing the number of Lagrange expansion domains over the cross-section, which would lead to a piecewise interpolation of the mechanical variables on the xz-plane, enabling the model to capture more complex deformations. The same can also apply to the HLE theories, but, in these models, the hierarchical characteristics of the expansion terms allow one to easily
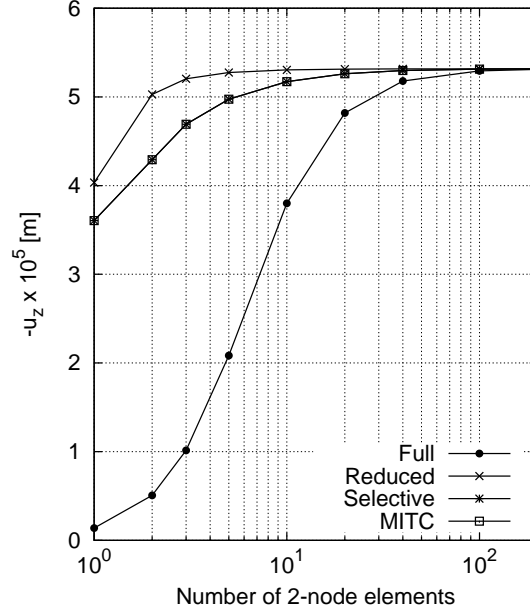
18

Figure 6: Vertical displacement, u_z, at the tip of the square beam for an increasing number of 2-node elements and the different integration schemes considered.

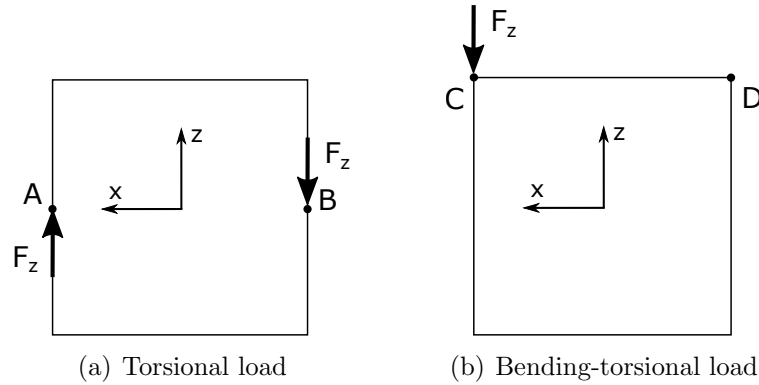(a) Torsional load   (b) Bending-torsional load

Figure 7: Tip cross-section for the different load cases.

enrich the kinematics by only increasing the polynomial order. Thanks to this capability, HLE can provide very accurate solutions with no need of cross-section refinements.

Another load case is considered to study the behavior of the present model under bending-torsion. To achieve this scope, a single point load with a magnitude of $F_z = 50$ N is applied at the left top corner of the cross-section, see Fig. 7 (b). Table 3 shows the solutions for the vertical displacements and maximum shear stresses at different evaluation points. Again, the results obtained from LE and HLE models are compared against analytical, classical and Taylor-based theories from [39]. The analytical formulas for pure-bending, shear and torsion have been already included in the previous section (Eqs. (35), (36) and (38)). The results show that the use of MITC beam elements, together with high-order expansions over the xz-plane, leads to models that are able to capture the actual deformation of the structure and the accurate state of stress under different load conditions.

19

Model	$u_z \times 10^6$ m at y=L	$\sigma_{yz} \times 10^3$ MPa at y=L/2	DOFs
Analytical	0.315	6.009	-
TE models [39]			
6-DOF	0.266	3.750	126
N=1	0.271	3.750	189
N=2	0.274	3.750	1818
N=3	0.285	3.750	3030
N=4	0.332	6.168	4545
N=5	0.345	6.168	6363
LE models			
L4	0.273	3.747	1212
L9	0.278	3.750	2727
HLE models			
HL1	0.273	3.747	1212
HL2	0.278	3.748	2424
HL3	0.331	6.167	3636
HL4	0.335	6.164	5151
HL5	0.345	6.069	6969

Table 2: Results of vertical displacements, u_z, and shear stresses, σ_{yz}, at Point A obtained with MITC2 elements for various theories of structures. Square beam under torsional load.

4.3 Asymmetric laminated beam

The numerical error introduced by the shear locking can be of major importance when dealing with laminated structures, in which an accurate description of the stress/strain state is of fundamental importance for verification purposes. In this context, a cantilever beam consisting in a two-layer asymmetric $[0°, 90°]$ cross-ply is considered in this section. This structural problem, represented in Fig. 8, was already studied by Pagani *et al.* [54]. The geometrical dimensions are: $b = 0.2$ m, $h = 0.1$ m and $L = 2$ m. Both laminae have the same thickness, equal to $h/2$, and the material properties, given in a dimensionless form, are: $E_L/E_T = 25$, $\nu_{LT} = \nu_{TT} = 0.25$, $G_{LT}/G_{TT} = 0.25$, where the subscript L correspond to the fiber direction and T refer to the normal direction. The beam is loaded at the free-tip with four point forces of the same magnitude, $F_z = 25$ N, as shown in Fig. 8.

The present assessment is focused on the effects of the longitudinal mesh discretization and the integration scheme on the goodness of the solutions, with a focus on the shear components of the stress field. First, a distribution of 4 quadratic beam elements (B3) is employed along the beam axis and the different integration schemes are accounted for. A layer-wise method is employed to describe the cross-section, using one expansion domain of fifth-order (HL5) per layer. The results of displacements and stresses at various points are shown in Table 4, together with solid element solutions obtained with the commercial software MSC Nastran, used here as a reference. The solid model is generated with a mesh of 8-node brick elements (HEX8) with a distribution of 10 elements per layer through-the-thickness direction. Figure 9

Model	$-u_z \times 10^5$ m at Point C, y=L	$-u_z \times 10^5$ m at Point D, y=L	$-\sigma_{yz} \times 10^3$ MPa y=L/2
Analytical solutions			
Pure bending	1.333	1.333	0
+ shear	1.342	1.342	1.875
+ torsion	1.358	1.326	4.879
Classical models [39]			
EBBM	1.333	1.333	0
TBM	1.342	1.342	1.250
TE models [39]			
6-DOF	1.355	1.329	3.125
N=1	1.382	1.355	3.125
N=2	1.344	1.314	3.358
N=3	1.350	1.316	4.008
N=4	1.358	1.315	5.217
N=5	1.363	1.315	5.271
LE models			
L4	1.130	1.101	3.125
L9	1.349	1.316	3.461
HLE models			
HL1	1.130	1.101	3.125
HL2	1.348	1.315	3.461
HL3	1.355	1.312	5.217
HL4	1.360	1.315	5.221
HL5	1.364	1.315	5.224

Table 3: Results of vertical displacements, u_z, and shear stresses, σ_{yz}, obtained with MITC2 elements for various theories of structures. Square beam under bending-torsional load
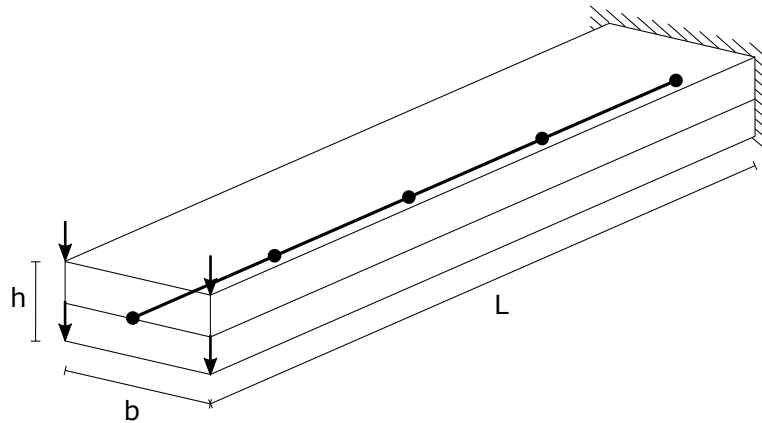

Figure 8: Structural problem of the asymmetric laminated beam.

Element	$-u_z \times 10^3$ m $[0, L, h/2]$	$\sigma_{yy} \times 10^{-3}$ [Pa] $[0, L/2, h/2]$	$-\sigma_{yz} \times 10^{-3}$ [Pa] $[0 , L/2, h/2]$	$-\sigma_{yz} \times 10^{-3}$ [Pa] $[0 , L/2, -h/4]$	DOFs
		MSC Nastran solid model			
HEX8	3.483	93.306	0.225	11.376	132300
		HL5 beam model			
B3 Full	3.468	84.480	0.466	16.783	1080
B3 Reduced	3.483	117.492	25.082	16.713	1080
B3 Selective	3.477	96.553	14.033	16.916	1080
MITC3	3.477	96.553	0.074	11.523	1080

Table 4: Deflections and stresses of the asymmetric laminated beam.

shows the distribution of shear stresses along the z-axis of the midspan section for all models considered. The following statements can be summarized from the results:

- The reduced integration provides optimum results in terms of displacements, minimizing the stiffening effects caused by the shear locking even for the coarse mesh employed in this case. On the other hand, it clearly overestimates both normal and shear stresses.

- Both the displacement solutions and the normal stresses show lower values when full integration is utilized. Again, the shear stresses are overestimated over the entire thickness of the lay-up, as shown in Fig. 9.

- Selective integration provides good results for displacements and normal stresses, although it is clear that the convergence of the solutions is not assured by employing only 4 cubic beam elements. The drawback of these beam elements resides on the computation of the shear stresses, which show an erratic distribution due to the error introduced in the numerical calculation of the integrals of the shear components of the stiffness matrix.

- The MITC method solves this issue by interpolating the shear components independently using lower-order shape functions. As a consequence, the structural model is capable of representing the exact distribution of shear stresses and, at the same time, the accuracy of the displacement solutions is preserved.

The use of reduced (and selective) integration methods to minimize shear locking phenomena can lead to significant errors in the computation of the shear components of the strain and stress tensors, even when the convergence of the primary solutions is satisfied. To address this issue, a convergence analysis is carried out using cubic selective beam elements (see Fig. 10 (a)) and the transverse shear stresses are compared for the four most refined models. Figure 10 (b) shows the distribution of shear stresses, σ_{yz}, along the top surface of the beam for 7, 10, 14 and 21 beam elements. In order to respect the stress-free conditions, σ_{yz} should have a constant value of zero over the top and bottom faces of the laminate. Instead, it is possible to observe that these values highly oscillate at the edges of the beam and how the error is
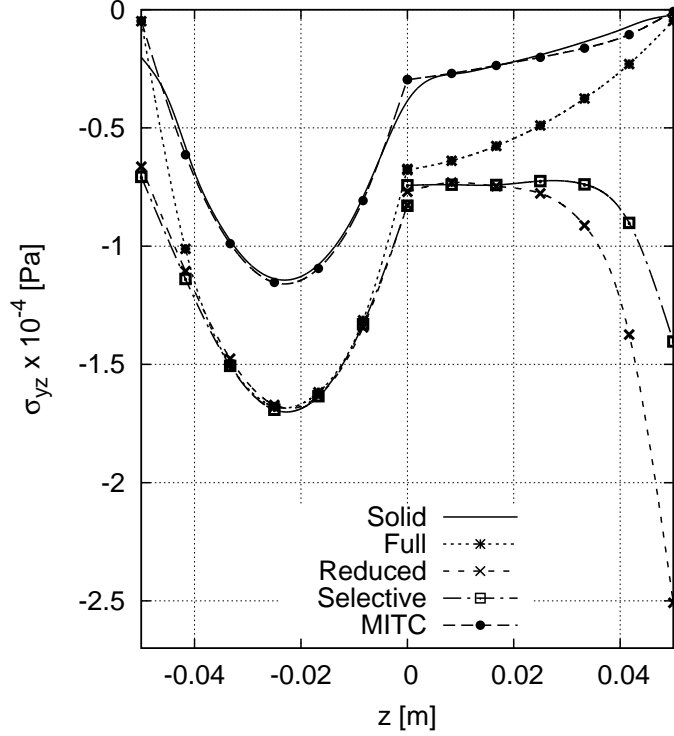
Figure 9: Shear stress, σ_{yz}, along the z-axis at midspan for four 3-node elements (HL5 model).

propagated towards the center. This erratic behavior is only mitigated when refining the finite element mesh (21 B4 selective), therefore adding considerable computational costs to the model. It should be also added that this numerical problem is even more noticeable when low-order elements are employed. The MITC method solves this issue without unnecessarily increasing the size of the mesh. Fig. 11 shows how MITC elements eliminate almost entirely these unwanted oscillations of σ_{yz} already for 7 beam elements, assuring the best accuracy of the stress solutions while keeping the computational efforts much reduced.

4.4 L-angle beam

CUF beam models are suited for the study of structural problems with 3D-like capabilities regardless of the complexity of the geometry. In this context, a thin-walled L-angle cantilever beam with a curved section is considered, with a focus of the enhanced capabilities of the MITC beam element for the efficient computation of displacement and stress solutions. The geometrical dimensions are shown in Fig. 12 (a), where $h = 20$ mm, $h_1 = 15$ mm, $t = 2$ mm and the outer radius $r = 5$ mm. The length of the beam, L, is 1 m, being the slenderness ratio as high as $L/h = 50$. A typical Aluminum alloy is employed for the material characteristics: Young modulus, E, equal to 75 GPa, and Poisson ratio, $\nu = 0.33$. A vertical force of magnitude $F = -50$ N is applied at point C of the tip section (see Fig. 12 (a)).

The beam axis has been discretized with 10 four-node beam elements and the cross-section surface is modelled with three expansion domains, as shown in Fig. 12 (b). The use of a non-isoparametrical mapping technique on the HLE high-order models, introduced by Pagani *et*
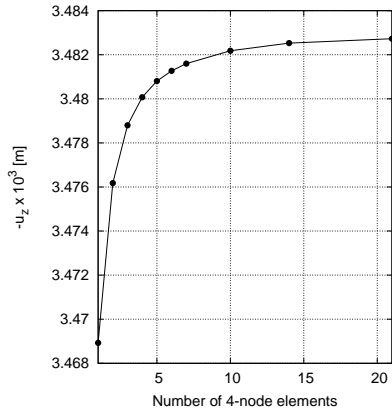
(a) Vertical displacement, u_z
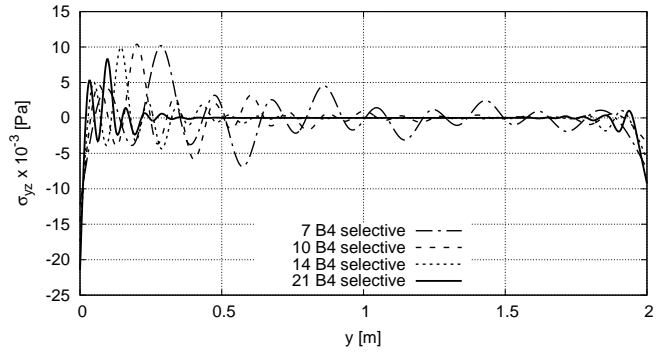
(b) Shear stress, σ_{yz}

Figure 10: Convergence analysis of the cross-ply beam for an increasing number of 4-node beam elements with selective integration (a) and transverse shear stress distribution at the top face along the beam axis (b) for the four most refined discretizations analyzed in (a).
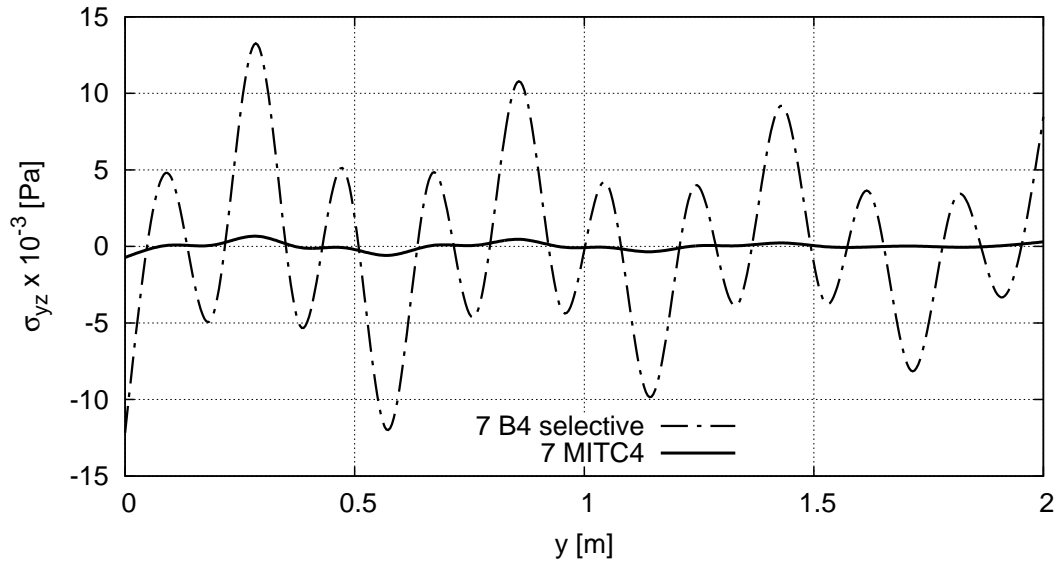

Figure 11: Shear stress, σ_{yz}, at the center of the top face along the cross-ply for seven selective B4 and MITC4 elements. HL8 beam model.

24

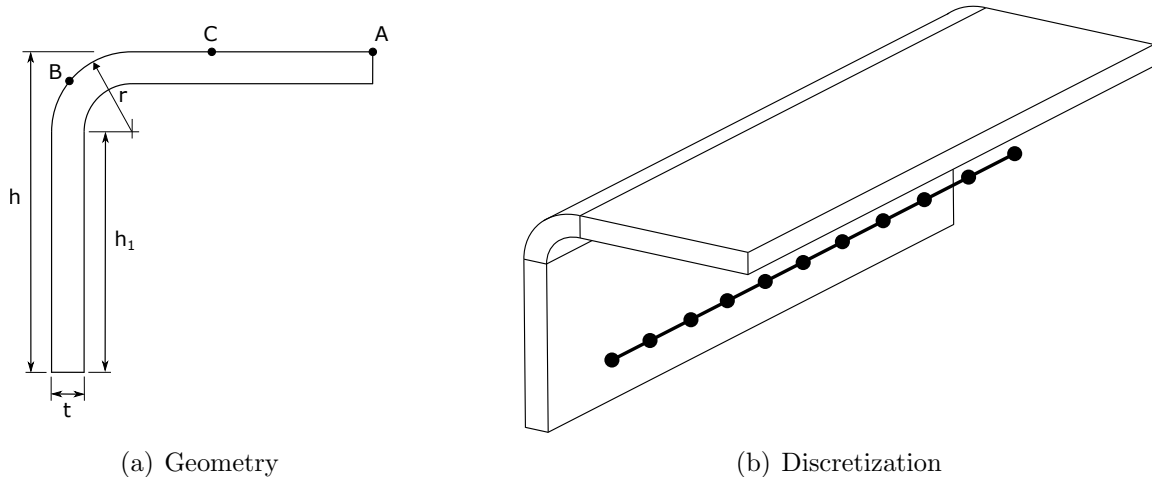| (a) Geometry | (b) Discretization |

Figure 12: L-angle beam model.

al. [55], allows one to capture the exact shape of curved sections with no geometrical error induced. Table 5 addresses the results of displacements and stresses at various points of the beam for all the integration methods considered in the present work. Third, fifth and seventh-order expansions over the cross-section are considered. Solutions obtained from beam, plate and solid models of MSC Nastran are also included as references. The 1D model in Nastran makes use of 20 2-node line elements (CBEAM), the 2D model employs a discretization of 28000 4-node plate elements (QUAD4), whereas 32000 8-node brick elements (HEX8) are used for the 3D model, including 4 elements in the through-the-thickness direction.

Similar conclusions to the previous examples can be extracted from this assessment. The reduced integration provides accurate results in terms of displacements, but it lacks on representing correctly the stress solutions. Full and selective integrations can be also used to compute the normal components of the stress field within an acceptable margin of accuracy. However, this study confirms that to obtain reliable solutions of the whole state of stress of the structure, MITC elements shall be employed. This statement is further supported in Fig. 13, which shows the transverse shear stress distribution across the thickness at point B at two sections of the beam, located at $y = 0.1L$ and $y = 0.5L$. It is possible to see that, unlike the conventional integration schemes, MITC element solutions are in good agreement with the solid ones, while keeping the computational costs much lower.

5 Conclusions

This paper has introduced a class of locking-free unified beam elements that show an outstanding performance in cases where common isoparametric finite elements fail. The Mixed Interpolation of Tensorial Components (MITC) method has been employed to overcome the shear locking problem and the Carrera Unified Formulation is exploited to generate various refined beam models with 3D-like capabilities. Moreover, the mixed interpolation of transverse shear strains, together with the use of higher-order approximations of the mechanical

25

Model	$u_z \times 10^1$ m	$\sigma_{yy} \times 10^{-8}$ Pa	$\sigma_{yz} \times 10^{-6}$ Pa	DOFs
	Point A, $y = L$	Point B, $y = 0.1$ m	Point B, $y = 0.1$ m	
MSC Nastran models				
CBEAM	-1.388	0.680	-	120
QUAD4	-1.431	2.123	6.253	43750
HEX8	-1.419	2.108	5.562	128000
Full integration - HLE CUF models				
HL3	-1.406	2.066	8.215	2604
HL5	-1.407	2.019	8.035	5301
HL7	-1.407	2.019	8.404	9114
Reduced integration - HLE CUF models				
HL3	-1.416	1.115	24.393	2604
HL5	-1.417	1.021	30.287	5301
HL7	-1.417	1.010	30.823	9114
Selective integration - HLE CUF models				
HL3	-1.407	2.072	12.643	2604
HL5	-1.408	2.031	13.844	5301
HL7	-1.408	2.029	14.088	9114
MITC integration - HLE CUF models				
HL3	-1.407	2.072	6.286	2604
HL5	-1.408	2.031	5.282	5301
HL7	-1.408	2.029	5.766	9114

Table 5: Results of displacements and stresses of the L-angle beam with 10 4-node elements.
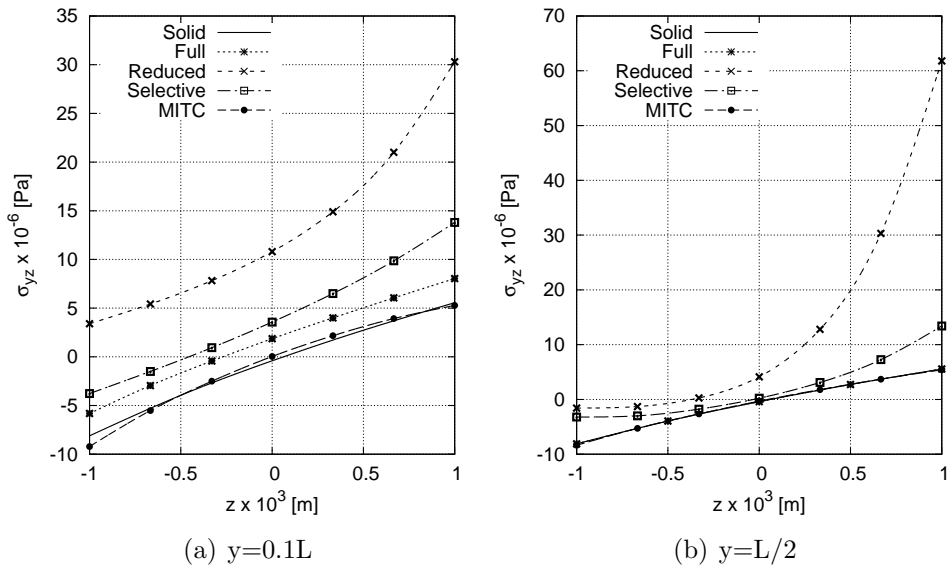

(a) y=0.1L

(b) y=L/2

Figure 13: Shear stress, σ_{yz}, distribution across the thickness at point B.

variables, has demonstrated to be a powerful tool to obtain highly accurate strain and stress solutions. The numerical examples carried out for this work suggest that the following comments on the capabilities of MITC beam models can be stated:

- Although the introduction of mixed interpolated beam elements might not represent a drastic improvement on the convergence rates of the displacement solutions in comparison with reduce/selective integration schemes, it has been proven that its use is necessary when an accurate description of the complete state of stress is required.

- High-order MITC beam elements have been successfully tested and assessed on various structural problems featuring different geometries and loading cases, proving to be a reliable tool to obtain 3D-like solutions with a considerable reduction of the computational costs.

- The formulation of this class of finite elements does not require the addition of new unknowns to the structural problem since the problem matrices remain formally the same. Therefore it represents a natural solution to tackle the shear locking problem from its source with no need of artificial numerical techniques, while also maintaining the efficiency of the beam models. These characteristics make the MITC method recommended for any isoparametric beam finite elements.

Acknowledgements

References

[1] T.H.H. Pian. Derivation of element stiffness matrices by assumed stress distributions. *AIAA Journal*, 2(7):1333–1336, 1964.

[2] J. N. Reddy. A penalty plate-bending element for the analysis of laminated anisotropic composite plates. *International Journal for Numerical Methods in Engineering*, 15(8):1187–1206, 1980.

[3] J. N. Reddy. On locking-free shear deformable beam finite elements. *Computer Methods in Applied Mechanics and Engineering*, 149:113–132, 1997.

[4] T. Belytschko, H. Stolarski, W.K. Liu, N. Carpenter, and Ong J.S.-J. Stress projection for membrane and shear locking in shell finite elements. *Comput. Methods Appl. Mech. Engrg*, 51:221258, 1985.

[5] T.J.R. Hughes and M. Cohen. The 'heterosis' finite element for plate bending. *Computers & Structures*, 9(5):445 – 450, 1978.

[6] M.A. Crisfield. A quadratic Mindlin element using shear constraints. *Computers & Structures*, 18(5):833 – 852, 1984.

[7] A. Tessler and S.B. Dong. On a hierarchy of conforming Timoshenko beam elements. *Computers & Structures*, 14(3):335 – 344, 1981.

[8] R.L. Spilker and N.I. Munir. The hybrid-stress model for thin plates. *International Journal for Numerical Methods in Engineering*, 15(8):1239–1260, 1980.

[9] K.C. Park and D.L. Flaggs. A symbolic fourier synthesis of a one-point integrated quadrilateral plate element. *Computer Methods in Applied Mechanics and Engineering*, 48(2):203 – 236, 1985.

[10] K.-Y. Yuan, Y.-S. Huang, and T. H. H. Pian. New strategy for assumed stresses for 4-node hybrid stress membrane element. *International Journal for Numerical Methods in Engineering*, 36(10):1747–1763, 1993.

[11] O. C. Zienkiewicz, R. L. Taylor, and J. M. Too. Reduced integration technique in general analysis of plates and shells. *International Journal for Numerical Methods in Engineering*, 3(2):275–290, 1971.

[12] M. Zlámal. Superconvergence and reduced integration in the finite element method. *Mathematics of Computation*, 32(143):663–685, 1978.

[13] G. Prathap and G. R. Bhashyam. Reduced integration and the shear-flexible beam element. *International Journal for Numerical Methods in Engineering*, 18(2):195–210, 1982.

[14] O.C. Zienkiewicz and E. Hinton. Reduced integration, function smoothing and non-conformity in finite element analysis (with special reference to thick plates). *Journal of the Franklin Institute*, 302(5):443 – 461, 1976.

[15] J. Barlow. More on optimal stress points reduced integration, element distortions and error estimation. *International Journal for Numerical Methods in Engineering*, 28(7):1487–1504, 1989.

[16] W.P. Doherty and R.L. Wilson, E.L. Taylor. Stress analysis of axisymmetric solids utilizing higher order quadrilateral finite elements. *Structural Engineering Laboratory, University of California, Berkeley, CA*, 1969.

[17] T.J.R. Hughes, M. Cohen, and M. Haroun. Reduced and selective integration techniques in the Finite Element Analysis of plates. *Nuclear Engineering and Design*, 46(1):203 – 222, 1978.

[18] D.S. Malkus and T.J.R. Hughes. Mixed finite element methods reduced and selective integration techniques: A unification of concepts. *Computer Methods in Applied Mechanics and Engineering*, 15(1):63 – 81, 1978.

[19] R.H. MacNeal and R.L. Harder. A proposed standard set of problems to test finite element accuracy. *Finite Elements in Analysis and Design*, 1(1):3 – 20, 1985.

[20] E.N. Dvorkin and K.J. Bathe. A continuum mechanics based four-node shell element for general non-linear analysis. *Engineering Computations*, 1(1):77–88, 1984.

[21] R.H. MacNeal. Derivation of element stiffness matrices by assumed strain distributions. *Nuclear Engineering and Design*, 70(1):3 – 12, 1982.

[22] M.J. Turner, R.W. Clough, H.C. Martin, and L.J. Topp. Stiffness and deflexion analysis of complex structures. *Journal of the Aeronautical Sciences*, 23(9):805–823, 1956.

[23] KJ. Bathe. *Finite element procedures*. Upper Saddle River, New Jersey: Prentice Hall, 1996.

[24] M.L. Bucalem and KJ. Bathe. *The Mechanics of Solids and Structures - Hierarchical Modeling and the Finite Element Solution*. Springer, 2011.

[25] M.L. Bucalem and K.-J. Bathe. Higher-order MITC general shell elements. *International Journal for Numerical Methods in Engineering*, 36(21):3729–3754, 1993.

[26] K-J. Bathe and E. N. Dvorkin. A formulation of general shell elementsthe use of mixed interpolation of tensorial components. *International Journal for Numerical Methods in Engineering*, 22(3):697–722, 1986.

[27] H. C. Huang and E. Hinton. A new nine node degenerated shell element with enhanced membrane and shear interpolation. *International Journal for Numerical Methods in Engineering*, 22(1):73–92, 1986.

[28] K.C. Park and G.M. Stanley. A curved C^0 shell element based on assumed natural-coordinate strains. *Journal of Applied Mechanics*, 53(2):278–290, 1986.

[29] J. Jang and P. M. Pinsky. An assumed covariant strain based 9-node shell element. *International Journal for Numerical Methods in Engineering*, 24(12):2389–2411, 1987.

[30] L. Euler. *De curvis elasticis*. Lausanne and Geneva: Bousquet, 1744.

[31] S. P. Timoshenko. On the transverse vibrations of bars of uniform cross section. *Philosophical Magazine*, 43:125–131, 1922.

[32] R.K. Kapania and S. Raciti. Recent advances in analysis of laminated beams and plates, part I: Shear effects and buckling. *AIAA Journal*, 27(7):923–935, 1989.

[33] R.K. Kapania and S. Raciti. Recent advances in analysis of laminated beams and plates, part II: Vibrations and wave propagation. *AIAA Journal*, 27(7):935–946, 1989.

[34] E. Carrera, A. Pagani, M. Petrolo, and E. Zappino. Recent developments on refined theories for beams with applications. *Mechanical Engineering Reviews*, 2(2):1–30, 2015.

[35] E. Carrera. Theories and finite elements for multilayered, anisotropic, composite plates and shells. *Archives of Computational Methods in Engineering*, 9(2):87–140, 2002.

[36] E. Carrera. Theories and finite elements for multilayered plates and shells: a unified compact formulation with numerical assessment and benchmarking. *Archives of Computational Methods in Engineering*, 10(3):216–296, 2003.

[37] E. Carrera and G. Giunta. Refined beam theories based on Carrera's unified formulation. *International Journal of Applied Mechanics*, 2(1):117–143, 2010.

[38] E. Carrera and M. Petrolo. Refined beam elements with only displacement variables and plate/shell capabilities. *Meccanica*, 47(3):537–556, 2012.

[39] E. Carrera and A. Pagani. Evaluation of the accuracy of classical beam FE models via locking-free hierarchically refined elements. *International Journal of Mechanical Sciences*, 100:169–179, 2015.

[40] P.-S. Lee, H.-C. Noh, and C.-K. Choi. Geometry-dependent MITC method for a 2-node iso-beam element. *Structural Engineering and Mechanics*, 29(2):2203–221, 2008.

[41] J. N. Reddy. A simple higher-order theory for laminated composites. *Journal of Applied Mechanics*, 51:745–752, 1986.

[42] E. Carrera, M. Cinefra, E. Zappino, and M. Petrolo. *Finite Element Analysis of Structures Through Unified Formulation*. John Wiley and Sons, Ltd, 2014.

[43] E. Carrera, M. Petrolo, and E. Zappino. Performance of CUF approach to analyze the structural behavior of slender bodies. *Journal of Structural Engineering*, 138(2):285–297, 2012.

[44] E. Carrera, A. Pagani, and M. Petrolo. Use of Lagrange multipliers to combine 1D variable kinematic finite elements. *Computers & Structures*, 129:194–206, 2013.

[45] E. Carrera and A. Pagani. Analysis of reinforced and thin-walled structures by multi-line refined 1D/beam models. *International Journal of Mechanical Sciences*, 75:278–287, 2013.

[46] E. Carrera, M. Maiarù, and M. Petrolo. Component-wise analysis of laminated anisotropic composites. *International Journal of Solids and Structures*, 49:1839–1851, 2012.

[47] E. Carrera, A. Pagani, and M. Petrolo. Component-wise method applied to vibration of wing structures. *Journal of Applied Mechanics*, 80(4):041012, 2013.

[48] E. Carrera, A. Pagani, and M. Petrolo. Classical, refined and component-wise theories for static analysis of reinforced-shell wing structures. *AIAA Journal*, 51(5):1255–1268, 2013.

[49] E. Carrera, A. Pagani, and M. Petrolo. Refined 1D finite elements for the analysis of secondary, primary, and complete civil engineering structures. *Journal of Structural Engineering*, 141(4):art. no. 04014123, 2014.

[50] E. Carrera and A. Pagani. Free vibration analysis of civil engineering structures by component-wise models. *Journal of Sound and Vibration*, 333(19):4597–4620, 2014.

[51] E. Carrera, A. Pagani, and R. Jamshed. Refined beam finite elements for static and dynamic analysis of hull structures. *Comput. Struct.*, 167(C):37–49, April 2016.

[52] E. Carrera, A.G. de Miguel, and A. Pagani. Hierarchical one-dimensional finite elements based on Legendre polynomial expansions. 2016. Submitted.

[53] B. Szabó and I. Babuka. *Finite Element Analysis*. John Wiley and Sons, Ltd, 1991.

[54] A. Pagani, A.G. de Miguel, M. Petrolo, and E. Carrera. Analysis of laminated beams via unified formulation and Legendre polynomial expansions. *Composite Structures*, pages –, 2016. In Press.

[55] A. Pagani, A.G. de Miguel, and E. Carrera. Cross-sectional mapping for refined beam elements with applications to shell-like structures. 2016. submitted.

[56] J. N. Reddy. *Mechanics of laminated composite plates and shells. Theory and Analysis.* CRC Press, 2nd edition, 2004.

[57] J. Barlow. Optimal stress locations in finite element models. *International Journal for Numerical Methods in Engineering*, 10(2):243–251, 1976.

[58] A. Higdon, E. Ohlsen, W.B. Stiles, J.A. Weese, and W.F. Riley. *Mechanics of materials.* 4th ed. New York: Jon Wiley & Sons, 1985.

A Stiffness matrix integrals

The integrals of the transverse expansions above the cross-section surface, E, are defined as:

$$E_{\tau,x s,x} = \int_\Omega F_{\tau,x} F_{s,x}\, d\Omega, \quad E_{\tau,z s,z} = \int_\Omega F_{\tau,z} F_{s,z}\, d\Omega, \quad E_s^\tau = \int_\Omega F_\tau F_s\, d\Omega,$$

$$E_{\tau,x s,z} = \int_\Omega F_{\tau,x} F_{s,z}\, d\Omega, \quad E_{\tau,z s,x} = \int_\Omega F_{\tau,z} F_{s,x}\, d\Omega, \quad E_{\tau,x s} = \int_\Omega F_{\tau,x} F_s\, d\Omega, \tag{39}$$

$$E_{\tau s,x} = \int_\Omega F_\tau F_{s,x}\, d\Omega, \quad E_{\tau,z s} = \int_\Omega F_{\tau,z} F_s\, d\Omega, \quad E_{\tau s,z} = \int_\Omega F_\tau F_{s,z}\, d\Omega,$$